Jurnal Teknologi

Full Paper

TiO_2-ENABLED POLYVYNYLIDENE FLUORIDE FOR PALM OIL MILL EFFLUENT TREATMENT: EFFECTS OF MEMBRANE MORPHOLOGY AND AERATION ON FLUX AND SUSPENDED SOLID REMOVAL

Erna Yuliwati[a*], Ahmad Fauzi Ismail[b], Goh Pei Sean[b], Sri Martini[a,c]

[a]Department of Chemical Engineering, Faculty of Engineering, Universitas Muhammadiyah Palembang, Jalan A. Yani 13 Ulu, 30251, Palembang, Indonesia
[b]Advanced Membrane Technology Research Centre Universiti Teknologi Malaysia, 81310 UTM Johor Bahru, Johor, Malaysia
[c]WA School of Mines: Minerals, Energy and Chemical Engineering, Curtin University, GPO Box U1987 Perth WA 6845, Australia

Article history
Received
28 April 2021
Received in revised form
17 October 2021
Accepted
9 November 2021
Published Online
20 December 2021

*Corresponding author
erna_yuliwati@um-palembang.ac.id

Graphical abstract

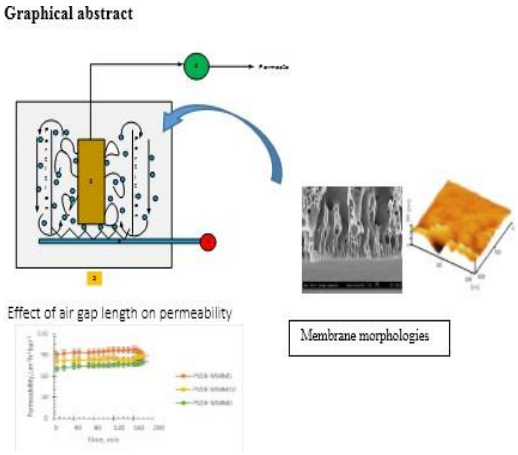

Abstract

A polyvinylidene fluoride-based mixed matrix membrane (PVDF- MMM) has been developed to treat palm oil mill effluent (POME). The addition of TiO_2 into PVDF membrane was conducted. Hollow fibers were spun from a dope solution containing PVDF/PVP 30K/DMAc/additives by using a dry-jet wet spinning process at different air gaps. AFM image demonstrated that wet spun hollow fiber had a rougher outer surface than that of dry-jet wet spun fibers and exhibited symmetric cross-section structure. Experimental results showed that hydrophilicity of membranes increased with adding of TiO_2 particles and the varied air gap length influenced the characteristic of membrane pore size and outer membrane surface roughness. In addition, aeration could increase the turbulence and flux and reduce membrane fouling. The values of flux and suspended solids removal were 92.04 L/m2.hr and 94.86 %, respectively, with the varied aeration flow rate of 2.0, 3.0 and 4.0 mL/min and bubble size distribution of 4.0 µm. Overall, this study has proven that PVDF-based MMM could achieve expected performance for POME treatment.

Keywords: Surface wettability, bubbles flow rate, wastewater purification, air gap length, TiO_2

Abstrak

Membran campuran dari bahan *polyvinylidene fluoride* dengan mekanisme *mixed matrix membrane (PVDF-MMM*) telah dikembangkan dalam penelitian ini untuk mengolah limbah cair kelapa sawit. Penambahan TiO_2 dalam pembuatan membran PVDF diberlakukan. Hollow fibers dipintal dari larutan yang mengandung tambahan komposisi PVDF/PVP 30K/DMAc/additif melalui *proses dry-jet wet spinning* pada *air gap* yang berbeda. Gambar AFM menunjukan bahwa wet hollow fiber yang telah dipintal memiliki permukaan luar yang lebih kasar dan menunjukan struktur *symmetric cross-section*. Hasil eksperimen menunjukan bahwa tingkat *hydrophilicity* dari membran meningkat dengan penambahan partikel TiO_2 sebanyak 10% berat dari jumlah PVDF, selain itu variasi *air gap* juga dianalisis. Aerasi dibuktikan dapat meningkatkan tingkat turbulensi and fluks membran serta menurunkan *fouling* membran. Nilai

dari penurunan flux dan padatan tersuspensi secara berturut – turut adalah 92.04 L/m2.hr dan 94.86 %, dengan penyesuain laju alir aerasi yaitu 2.0, 3.0 dan 4.0 mL/min dengan ukuran gelembung 4.0 µm.

Kata kunci: Hidrofilik, laju alir gelembung, pengolahan limbah cair, air gap, TiO_2

1.0 INTRODUCTION

Indonesia is one of the largest palm oil producers providing most of global demand on palm oil product leading to the increase in its production rate [1, 2]. Consequently, the amount of undesirable palm oil mill effluent (POME) has also been increasing and caused a detrimental effect of both environment and human health. Palm oil industry produced two types of waste namely solid and liquid waste. Liquid waste known as POME is viscous liquid waste and high in colloidal suspension containing of water, oil, and total solids including suspended solids that causes the water pollutant [3, 5]. POME is generated mostly from sterilizer condensate, clarification condensate and hydro cyclone waste and has unpleasant odor with characteristics as stated in Table 1 [6]. Nowadays, most of the POME treatment uses the application of conventional biological technique, namely anaerobic facultative digestion [7-9]. However, this method needs higher operational cost and wider treatment place. It also generates vast amount of corrosive and hazard biogas.

Regarding this issue, membrane technology that has attracted an increasing interest from both academic circle and industry stakeholder can be chosen as one of reliable water remediation technologies as it offers higher purification level along with lower energy consumption and scalability [10]. However, membrane system has its main drawback namely membrane fouling that needs to be addressed well to lengthen its lifespan and reduce maintenance cost [11]. The main cause of membrane fouling is the accumulation of suspended solids, inorganic and organic pollutants on membrane pores and surface reducing the amount of feed or permeate to pass the membrane layer.

Table 1 POME Characteristic and standard discharge

Parameters	Type of POME	Standard discharge, mg/L	Concentration of pollution loading, mg/L
BOD5	25,000-29,000	100	225 (1.01)
COD	51,000-64,000	350	888 (0.25)
TSS	18,000-23,000	250	263 (1.02)
Oil and grease	6,000-7,000	25	63 (0.08)
Total nitrogen	750-1,200	50	21.5 (0.53)n
pH	4..5		6-9

Table 1 showed the data of characteristics and standard discharge of POME, which mentioned the parameters of pollutant concentration were higher than standard discharge. Therefore, the discussion of pollutant treatment was important, especially the use of membrane technology to treat the pollutant concentrations in wastewater of POME.

There have been several mitigation strategies available to overcome membrane fouling problems such as adjusting pH, ionic strength and reducing suspended solids concentration. Other than that, optimizing process condition including air bubble characteristics and aeration process can also be dependable alternatives [8, 12]. However, some aspects related to the effects of several modification techniques on membrane fabrication such as membrane composition, airgap length, post treatment, etc. have been studied by few researchers [9-13].

Therefore, in this current work, the fabrication of polymeric ultrafiltration membrane, which contains Polyvinylidene fluoride (PVDF), Polyvinyl pyrrolidone (PVP) as pore former and TiO_2 (Titanium dioxide) that affects the hydrophilic characteristic by using various air gap length differences (0, 3, and 5 cm) for treating POME was investigated. The objective of this study was analyzed the effect of air gap length on membrane morphology and filtration.

2.0 METHODOLOGY

2.1 Materials

Polymeric ultrafiltration membranes were prepared using Kynar®740 PVDF polymer pellets purchased from Arkema Inc. Philadelphia, USA. The solvent N, N-dimethylacetamide (DMAc Aldrich, Chemical) (Synthesis Grade, Merck, 99%) was used as polymer solvent without further purification. TiO_2 was purchased from Sigma-Aldrich. PVP was purchased from Merck (Germany). Glycerol was purchased from Merck (Germany) used as non-solvent for the post treatment of membrane. In all experiments, tap water was used as the external coagulation bath medium in the spinning process.

2.2 Preparation of PVDF Spinning Dopes

The measured amount of pre-dried PVDF pellets were poured into pre-weighed DMAc solvent, and they were

then stirred thoroughly prior to the addition of known amount of PVP at temperature of 50°C. Rutile TiO_2 was then added to the polymer dope mixture and stirred for around 48 h (IKA-20-W) at 500 rpm to obtain a homogenous solution. Furthermore, the polymer solution was kept in a glass bottle and the air bubbles formed in the dope were removed using water aspirator. The fully dissolved polymer solution was transferred to a stainless steel reservoir. It was then degassed for 24 h at room temperature prior to the spinning process. Solution viscosity was measured using rheometer (Bohlin Instrument Ltd.) at decided temperatures.

2.3 Preparation of Composite Membranes

PVDF hollow fiber ultrafiltration membranes were initially spun at room temperature using a dry-jet wet spinning method. Membranes were fabricated by employing PVDF 19 wt.% in DMAc, 10 wt.% TiO_2 and 4.0 wt.% PVP, which were maintained of the weight of the PVDF at different air gap length (0, 5, 10 cm), as shown in Table 2.

Table 2 Fabricated PVDF Membrane at different TiO_2 concentrations

PVDF (wt %)	PVP (wt %)	TiO_2 (wt %)	Code
19	4	10	PVDF-MMM0
19	4	10	PVDF-MMM5
19	4	10	PVDF-MMM10

The dope solution was pressurized through spinneret with controlled extrusion rate while the internal coagulant was adjusted at 1.3 mL/min. Air gap length was set up at 0, 3, 5 cm. The hollow fiber that emerged from the tip of spinneret was guided through the two water baths at a take up velocity of 15.0 cm/s. Further, it was adjusted to suit the free-falling velocity. The spun hollow fibers were immersed in the water bath for three days. The hollow fibers were then post-treated using 10 wt.% glycerol solutions for 24 h. After the fibers were dried, they then were ready for making hollow fiber test module.

The experimental work of POME treatment process using polymeric membrane composite conducted in this study can be seen in Figure 1 [14]. Prepared suspension in membrane reservoir has volume of 9 L. The crossflow stream was produced by air bubbling generated by a diffuser. The air bubbling flow rate per unit projection membrane area was set at 2.0, 3.0 and 4.0 mL/min in order to produce proper turbulence. The filtration pressure was supplied by a vacuum pump and controlled by a needle valve. Bubble size generation was adjusted using different aerators having diameter within the range of 4 μm. Eventually, permeate flow rates were periodically measured using flow meter.

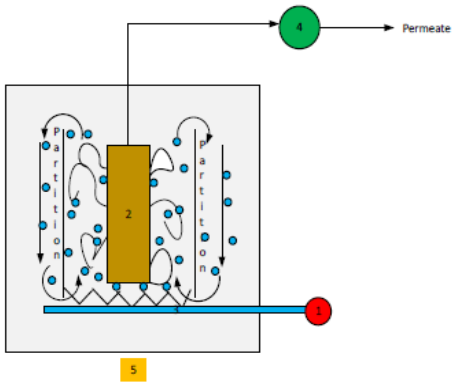

Figure 1 Schematic representation of ultrafiltration membrane for palm oil wastewater: (1) aerator; (2) membrane; (3) generated bubble; (4) pump; (5) membrane reservoir

2.4 Scanning Electron Microscopy (SEM)

The analysis of membrane morphology was performed by utilizing SEM (S-800M, Hitachi High Technology Co. Ltd., Tokyo, Japan). In order to observe membrane cross sections, membranes were frozen in liquid nitrogen. All sample sections then were sputter-coated with a thin gold film prior to SEM examination.

2.5 Atomic Fourier Microscope (AFM)

Membrane surface was characterized by AFM using tapping mode nanoscope III equipped with a 1553D scanner (SPA-300 HV, USA). All samples were washed using ethanol solution to remove all traces. Small pieces were cut from each membrane to be suited into magnetic disks using double side adhesive tape and then attached to a magnetic sample holder following procedures that was stated in the previous publication [15, 16]. As resistance of Rc and Ra can be generally removed using tap water flushing and chemical cleaning, respectively. The individual resistance due to different mechanism can be calculated using the following equations.

$$R_m = \frac{\Delta P}{\mu J_{wF}} \quad (1)$$

$$R_{cp} = \left(\frac{\Delta P}{\mu J_a}\right) \quad (2)$$

$$R_c = \left(\frac{\Delta P}{\mu J_c}\right) - R_m - R_{cp} \quad (3)$$

$$R_a = \left(\frac{\Delta P}{\mu J_{cp}}\right) - R_m - R_{cp} - R_c \quad (4)$$

where JwF is the initial water flux (m/s). the water flux after removing the cake layer by flushing with tap water for 10 mons (m/s), Ja is the water flux after 10 mins of chemical cleaning with a 0.1 M HCl solution (m/s) and Jcp is the flux of humic acid at the end of filtration (m/s).

2.6 Hydrophilicity

The hydrophilic nature of the surface membrane was illustrated by an optical camera using an Attention Theta T200 blood pressure monitor (Bolin Scientific, Sweden). The measurements were performed using ultrapure water drop (5µL). For all membranes, at least three measurements were conducted. The average value and the corresponding standard deviation were then calculated.

2.7 Membrane Pore Diameter and Porosity

In this work, the bubbles affecting membrane pore diameter were generated by tubular SS pipe under liquid cross-flow of 2.0, 3.0 and 4.0 mL/min with ratio of transmembrane (TMP/bubble point (BP) equal to 1.1. Membrane porosity (ε %) which refers to the ratio between volume of membrane void sites and the overall membrane voids sites and the overall membrane volume was examined using gravimetric method [17] as expressed by the following formula.

$$\varepsilon(\%) = \left\{ \frac{(Ww - Wd)/\rho_i}{(Ww - Wd)/\rho i + \frac{Wd}{\rho P}} \right\} \quad (5)$$

where ε, Ww, WD and ρi are membrane porosity (%), the weight of wet membrane, the weight of the dry membrane, and the kerosene density (0.82 g.cm^{-3}), respectively. Membrane hydrophilicity can be calculated by determining the value of contact angle of a water droplet on the membrane surface [18-20]. Specifically, a wider distribution and greater bubble size could be observed when the contact angle was higher than 450 illustrating the force expanding the bubbles. A higher contact angle influences bubble expansion, therefore, membrane surface should be treated to reduce the value of contact angle. The contact angle has a significant influence on the detached bubble size depending on the wettability system [21].

2.8 Membrane Ultrafiltration

The experimental set up of permeation flux and retention rate of PVDF-MMM membrane study was illustrated in Figure 1. Specifically, the bundle of membrane having a filtration area of 16 cm2 was submerged in the prepared suspension in a membrane reservoir with a volume of 9 L. A cross-flow stream was produced by air bubbles (mean diameter of bubbles of 4 µm) generated by a diffuser located underneath the submerged membrane bundle for mechanical cleaning of the membrane surface. The air bubbling flow rate was set up at 2.0, 3.0, and 4.0 L/min which was periodically recorded using a flow meter. The flux and suspended solids removal was analyzed using synthetic POME (Table 2). All experiments were conducted at temperature 25 °C.

Table 2 Process conditions of POME treatment

Number	Factors	Values
A	Suspended Solids mg/L	
1		3.0
B	Air bubble flow rate, mL/min	
1		2.0
2		3.0
3		4.0
C	Bubble size generation, µm	
1		4

Pure water permeation flux (Jw) was measured at reduced pressure (0.5 bar absolute) on the permeate side. Then, the permeation flux for the POME (J) was measured and can be calculated as follows.

$$J = \frac{V}{A \Delta t} \quad (6)$$

where *J is* the flux (L/m^2 h), L is the permeate volume, A is the membrane surface area (m^2), and t is the time (h).

Suspended Solids Removal

Suspended solids (SS) removal was measured using a spectrofotometer (DR5000, HACH, Method 8000, TNT822, 20-1500 mg/L SS) according to the standard procedures. The formula of SS removal efficiencies can be written as follows.

$$\text{SS removal (\%)} = \left(\frac{SS0 - SS}{SS0}\right) \times 100 \quad (7)$$

where *SS0* and SS are the initial concentration of suspended solid in POME and permeate, respectively.

3.0 RESULTS AND DUSCUSSION

3.1 Effect of Air Gap Length

The PVDF-MMM membranes prepared at different air gap lengths (0, 3, and 5 cm) were analyzed using pure water flux. Figure 2 displays the SEM micrographs of PVDF-MMMs morphology related to the difference in air gap length. Based on the figure, it can be assumed that TiO_2 nanoparticles have high specific areas and hydrophilicity affecting on the mass transfer process during the spinning process [22]. Other than that, the pore size of membrane became larger with the increase in the airgap length from 0 to 5 cm as shown in Table 4. This phenomenon can be attributed to the shear-induced pore deformation and transformation from big pores to small pores due to the effects of elongation stress and interfacial stress on the inner and outer surface during spinning process and the difference of water-solution and air-solution interfaces [23]. In this case, the membrane pores could be

merged with each other to create larger pores when membrane surface has deep depression.

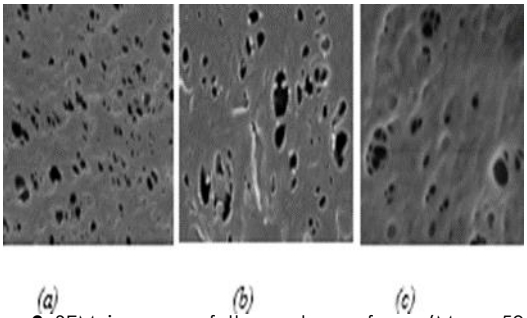

Figure 2 SEM images of the outer surface (Mag. 50.0kx) of PVDF-MMM with air gap length of (a) 0 cm; (b) 3 cm (c) 5 cm

Based on Figure 2, it can also be observed that the increase in air gap length could enhance contact time between the spun fibers and bore fluid. This finding was coherent with the previous study report [23]. Additionally, it was found that the outer membrane surface was smooth and dense.

Furthermore, air gap length could affect the average membrane deceased pore size diameter that increased from 0 cm to 5 cm (Table 3). Outer surface of prepared membrane PVDF-MMM at air gap 0, 3 and 5 cm were found to be in the axial direction of bore fluid flow. In addition, the wall thickness of membrane decreased from 0.24 mm to 0.19 mm due to the elongation of hollow fiber triggered by the gravity while it travels through the air gap. This can be caused by stretching force leading to thinner membrane material [24]. Other than that, the average nodules size was also affected by air gap length implying the imbalance of elongation and interfacial stresses during spinning process.

Table 3 Average poresize diameter and wall thickness of PVDF-MMM membranes at different air gap lengths

Air gap (cm)	Code/ OD, nm (s.d)	ID, nm (s.d)	Thickness, mm (s.d)
0	PVDF-MMMa 18.90 (0.09)	12.23 (0.01)	0.24 (0.10)
3	PVDF-MMMb 20.33 (0.35)	11.09 (0.13)	0.20 (0.09)
5	PVDF-MMMc 24.86 (0.08)	11.09 (0.09)	0.19 (0.06)

For better results, microscopic analysis was also conducted using AFM as seen in Figure 3. It is believed that the elongation stress caused by axial direction becomes more pronounced with the increasing air gap and can diminish membrane surface roughness due to molecular orientation induced by shear stress within the spinneret that might relax in the air gap region [24-26]. The elongation stress and the spin line are small due to viscoelastic fluid in spinning solution which increased when the spin line stress was high [25]. It can be concluded that the decrease of roughness parameters on the outer surface was affected by an increase in air gap length.

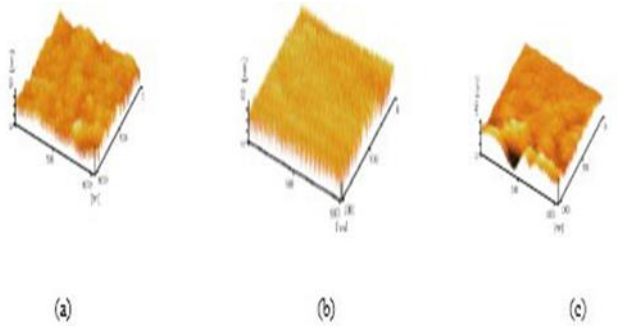

Figure 3 AFM images of outer surface PVDF-MMM (a) 0 cm; (b) 3 cm (c) 5 cm

3.2 Effect of TiO_2 Concentration

Generally, the permeability of PVDF membrane increases with adding the TiO_2 concentration in different air gap length influenced membrane pore size (Figures 4 and 5). In particular, Figure 4 showed the increase in the outer surface pore size which was influenced by the addition of 10 wt % of TiO_2 in varied air gap length. The cross- sectional images for all hollow fibers consist of finger- like macrovoids extending from both inner and outer wall of the hollow fiber to an intermediate sponge-like layer. The thickness of the sponge-like layer decreases with the increase air gap length from 0 to 10 cm (Figures 4a and 4c). This phenomenon can be linked to the elongation caused by axial direction. TiO_2 concentration in polymer membrane has been explained by previous studies that describe the kinetic effect on the rate of solvent-nonsolvent exchange in the phase inversion process tend to provide the higher hydrophilicity and smaller average pore size [22,26]. the increase in the length of finger-like macrovoids and the decrease in the thickness of the intermediate sponge-like layer were recognized. This has drawn a summary that the enriched surface hydrophilicity would lead to little improvement of permeability due to insignificant effect of concentration polarization [27].

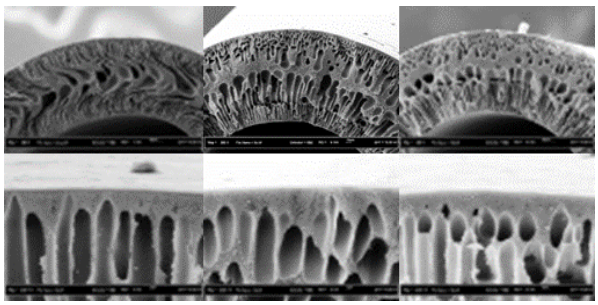

Figure 4 SEM images of outer surface PVDF-MMM of (a) PVDF-MMM0; (b) PVDF MMM3; (c) PVDF-MMM5

Table 4 summarizes membrane mean pore size on its external surface. There was a continuous increase in the membrane outer pore size with the air gap for all PVDF-MMM hollow fibers prepared by the dry/wet spinning technique. Specifically, the pores of PVDF-MMM10 membrane was blocked more seriously due to a lower porosity value while PVDF- MMM5 membrane still had more space for the solution to go through. This may be attributed to the elongation force parallel to fiber axis which has higher extent at high air gap length. This indicates that the membrane surface porosity is also an important factor affecting membrane fouling and the solute rejection.

This work then found that hydrophilicity values were similar among three membranes. The differences in the fouling value can be attributed to the differences in surface porosity and surface roughness of the membranes as stated in Table 4. Suspended solid molecules trapped on the membrane surface blocked membrane pores due to low porosity leading to membrane fouling. This indicates that the membrane surface porosity is a crucial factor influencing both membrane fouling and solute rejection.

Table 4 Pure water permeability (PWP) under different air gaps

Samples	Contact angle, θ(s.d)	Roughness, nm (s.d)	Average Poresize, nm (s.d)	Porosity, % (s.d)	PWP, L/m²hbar (s.d)
PVCF-MMM0	52.3 (0.23)	16.5 (0.08)	29.2 (0.31)	70.44 (0.02)	73.9 (0.06)
PVCF-MMM5	50.4 (0.30)	12.9 (0.05)	32.86 (0.10)	80.25 (0.05)	94.8 (0.20)
PVCF-MMM10	48.3 (0.10)	11.0 (0.03)	34.02 (0.42)	82.53 (0.10)	92.9 (0.03)

It was found that PWP of wet spun PVDF hollow fiber membranes could be higher than that of dry-wet spinning PVDF hollow fiber membranes. It linked to molecular orientation induced by shear stress within the spinneret that may be frozen into the fiber and relax in the small air gap area [23, 24]. This has caused smaller pore size and/or denser skin for wet spinning version leading to a lower flux. Based on air gap length of 5 cm could be sufficient for enhancing PVDF hollow fiber membranes performance in terms of its permeation flux [24]. It was also predicted that the increase in air gap length will directly influence the membrane pore size [28].

This work found that pore size of the outer surface of the wet spun fiber (PVDF-MMM0) is18.90 nm in which it is larger than both PVDF-MMM5 (20.33 nm) and PVDF-MMM10 (24.86 nm). This may be caused by the die swell of composite PVDF macromolecules at the exit spinneret related to membrane surface roughness. Other than that, PVDF-MMM0 membrane has higher permeability degree than that of PVDF- MMM5 and PVDF-MMM10 membranes. This condition effected the ability of PVDF-MMM0 in terms of higher SS removal due to having smaller membrane pore sizes as SS can form a cake layer on the membrane surface without the migration into the membrane pores affecting membrane permeability (Figure 5).

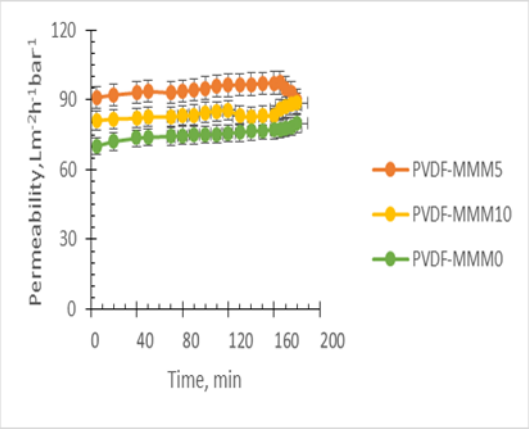

Figure 5 Membrane permeability as the function of time

3.3 Membrane Filtration Performance

Bubble Size Distribution

Bubble size distribution was measured using spraytec instrument (Malvern) used for the measurement of drop sizes from sprayer (Figure 6). In this work, bubble was generated by the aerator with the size of bubble 4 µm. Theoretically, membrane surface having contact angle, θ, more than 45 o could trapped larger bubbles with broad diameter distribution, and the increase in contact angle tends to increase both the mean bubble size and particle size dispersal coefficient [29]. Contact angle related to the interfacial tension can be used to understand the behaviour of this spesific solid-liquid interactions using Young's equation as expressed in Equation 5.

$$\gamma mw = \gamma mw + \gamma wg \cos \theta \quad (8)$$

Where γmw, γwg, and γmw are interfacial tension between water phase and membrane surface, surface tension between membrane surface and gaseous phase, and surface tension between surface membrane and water phase, respectively.

The shear stress on membrane surface could be evaluated by electrochemical shear method. The amplitude of the outer wall membrane shear stress was influenced by flux enhancement. However, this phenomenon had no effect on a flat sheet module. In the hollow fiber configuration, low average shear stress referred to the performance of hollow fiber dominated by standard deviation where the increasing axial flow (γwg) tended to decrease standard deviation of shear stress affecting fouling reduction [30].

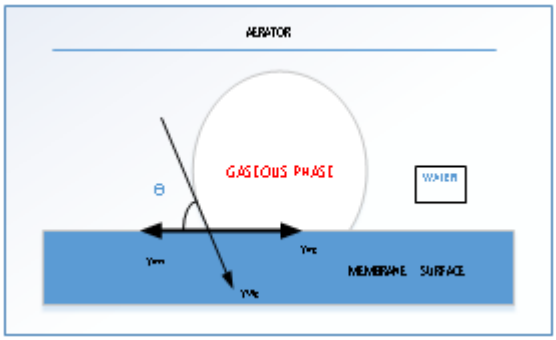

Figure 6 Schematic presentation of force balance at three phase linie of interfacial tension of bubble

Bubble Flow Rate

Bubble flow rate plays an important role in the aeration management affecting fouling reduction. This study detected that that the increase in bubbles flow rate could increase the flux rate and SS removal efficiency, especially by increasing the flowrate to 3.0 mL/min even though it can also be seen that the flux and suspended solids may decrease simultaneously due to smaller surface tension of membrane pores. There are some previous studies reported that the increase in membrane fouling happened due to the increasing SS concentration, however, some other studies showed different findings revealing no effect of suspended solids concentration on fouling beyond threshold concentration [28-30]. Other than that, it was believed that the continuous air flow rate could enhance the turbulence and membrane critical flux reducing membrane fouling rate, and this phenomenon can be attributed to the critical flux point of the membrane itself [31].

Figure 7 shows the trend of dP/dt for various bubbles flow rate. In the figure, significant variation was observed in terms of membrane permeability recovery as expressed by the recovery factor of dP/dt calculated during the hysteresis loops. The experimental data analysis showed that bubbles flow rate of 3.0 mL/min could enhance the flux better than that of bubbles flow rate of 2.0 and 4.0 mL/min. The supression degree of irreversible fouling occured at bubbles flow rate of 3.0 mL/min due to a higher flux.

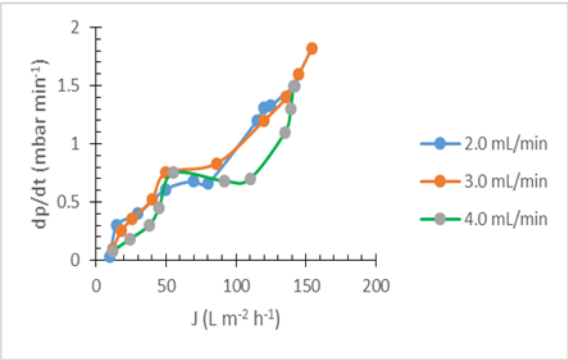

Figure 7 The effects of different specific bubble flow rates on permeate volume using PVDF-MMM5

This can be attributed to the aeration and air scouring processes. In this case, the measurement of storage Sauter diameter and zeta potential of nanobubbles were influenced by the flow rate of nanodispersions, and the stability of the bubbles was affected by dissolved gas concentration [32].

Eventually, this study found the best results of flux and suspended solids removal were 92.04 L/m^{2}h and 94.86%, respectively. It can be obtained by using PVDF-MMM5 membrane, air bubble flow rate, and bubble size generation values of 3.0 mL/min, and of 4.0 µm, respectively (Table 5).

Table 5 Removal of the main POME parameters

Parameters, Unit	Results
Flux, L/m^2.h	92.04
Suspended Solids Removal, %	94.86

4.0 CONCLUSION

This work has developed the submerged ultrafiltration membrane namely PVDF-MMMs fabricated via a dry-jet wet spinning method to investigate its performance referred to flux rate, fouling mechanism, membrane permeability and morphology when treating POME. Various concentrations of TiO_2 at constant value of PVP were used as inorganic additives in the spinning dopes in order to improve the phase-inversion rate and provide porous asymmetric membranes. Several characterizations and measurement techniques such as membrane structure, surface wettability, porosity, average pore size, and permeability were utilized to evaluate membrane structural details along with its performance. SEM analysis indicated that the addition of 5 wt.% TiO_2 nanoparticles resulted in smaller nanoparticles leading to higher hydrophilicity, small pore size, and high porosity. Moreover, permeability test indicated that PVP and TiO_2 nanoparticles positively affected the hydrophilic behavior of PVDF-MMMs. To conclude, higher flux rate (92.04 L/m2h) and total suspended solids removal (94.86%) could be achieved at optimum condition of air bubble flow rate of 2.0, 3.0 and 4.0 mL/min and bubbles size distribution of 4 µm, respectively.

Acknowledgement

This study was supported by Ministry of Higher Education of Republic Indonesia through a scientific research project (Project Number SP DIPA 388/h4/KPT.KP/2019). We thank to PTPN VII Betung for data resources and Advanced Membrane Technology and Research Center Universiti Teknologi Malaysia for membrane system and membrane samples. We are also grateful to Dr. Abid Djazuli, S. E. M. M from Universitas Muhammadiyah Palembang-Indonesia and Prof. Dr. Datuk Ts. Ahmad Fauzi Ismail from Universiti

Teknologi Malaysia-Malaysia for supporting the technical research.

References

[1] Ministry of Environmental of Republic Indonesia. 2017. Parameter Limits of Effluent.

[2] Abdulsalam, H. M., Che Man, H., Idris, A.I., Yunos, K. F., & Abidin, Z. Z. 2018. Treatment of Palm Oil Mill Effluent using Membrane Bioreactor: Novel Processes and Their Major Drawbacks. *Water*. 10(9): 1165-1211. DOI: https://doi.org/10.3390/w10091165.

[3] Paramitadevi, Y. Y. and Rahmatullah. 2017. Technical Problems of Wastewater Treatment in Crude Palm Oil Industry: A Case Study in PT Soefin Indonesia-Kebun Sungai Liput Naggroe Aceh Darussalam Province. *Journal of Earth and Environmental*. 65: 012048. DOI: 10.1088/1755-1315/65/1/012048

[4] Judd, S. 2006. *Principles and Applications of Membrane Bioreactors in Water and Wastewaters Treatment*. Elsevier, Oxford.

[5] Li, Q., Xu, Z.L. & Yu, L.Y. 2010. Effect of Mixed Solvents and PVDF Types on Performnaces of PVDF Microporous Membranes. *Journal of Applied Polymer Science*. 115: 2277-2287. DOI: https://doi.org/10.1002/app.31324.

[6] Jyothi, M. S., Nayak, V., Padaki, M., Balakrishna, R. G., & Soontarapa, K. 2016. Aminated Polysulfone/ TiO_2 Composite Membranes for an Effective Removal of Cr(VI). *Chemical Engineering Journal*. 283: 1494-1505. DOI: https://doi.org/10.1016/j.cej.2015.08.116.

[7] Wang, T., Yang, Y., Zheng, J., Zhang, Q. & Zhang, S. 2012. A Novel Highly Permeable Positively Charged Nanofiltration Membranes based on a Nanoporous Hypercrosslinked Polyamide Barrier Layer. *Journal Membrane Science*. 448: 180-189. DOI: ttps://doi.org/10.1016/j.memsci.2013.08.012.

[8] Buscio, V., Crespi, M., and Gutiérrez-Bouzan, C. 2016. Application of PVDF Ultrafiltration Membranes to Treat and Reuse Textile Wastewater. *Desalination and Water Treatment*. 57: 8090-8096. DOI: https://doi.org/10.1080/19443994.2015.1021854.

[9] Cao, X. C., Ma, J., Shi, X. H. & Ren, Z. J. 2006. Effect of TiO_2 Nanoparticle Size on the Performance of PVDF Membrane. *Applied Surface Science*. 253(4): 2003-2010. DOI: https://doi.org/10.1016/j.apsusc.2006.03.090.

[10] Tana, Y. H, Goh, P. S., Lai, G. S., Lau, W. J., & Ismail, A. F. 2014. Treatment Of Aerobic Treated Palm Oil Mill Effluent (AT-POME) by using TiO_2 Photocatalytic Process. *Jurnal Teknologi*. 70(2): 61-63. DOI: https://doi.org/10.11113/jt.v70.3436.

[11] Braak, E., Alliet, M., Schetrite, S., & Albasi, C. 2011. Aeration and Hydrodynamic in Submerged Membrane Bioreactors. *Journal of Membrane Science*. 379: 1-18. DOI: https://doi.org/10.1016/j.memsci.2011.06.004.

[12] Ulatowski, K., and Sobieszuk, P. 2018. Influence of Liquid Flowrate on Size of Nanobubbles Generated by Porous-Membrane Modules. *Chemical Proses Engineering*. 39(3): 335-345. DOI: https://doi.org/10.24425/122954.

[13] Mansourpanah, Y., and Momeni-Habili, E. 2015. Investigation the Separation Properties of TiO_2-TFC Nanocomposite Membranes by Comparing the Presence or Absence of UV Irradiation; Membrane Preparation and Characterization. *Journal of Membrane Science Research*. 1: 26-33.

[14] Yuliwati, E., Porawati, H., Elfidiah, & Melani, A. 2019. Performance of Composite Membrane for Palm oil Wastewater Treatment. *Journal of Applied Membrane Science & Technology*. 23(2): 1-10. DOI: https://doi.org/10.11113/amst.v23n2.147.

[15] Bazinet, L., Poulin, J. F., and Amiot, J. 2007. Effect of Conditioning Ultrafiltration Membranes on their Performances in Electrodialysis with Ultrafiltration Membrane. *Separation Science and Technology*. 42: 2501-2518. DOI: https://doi.org/10.1080/01496390701477089.

[16] Wang, Y. J., and Kim, D. J. 2007. Crystallinity, Morphology, Mechanical Properties and Conductivity Study of In Situ Formed PVDF/LiClO4/TiO_2 Nanocomposite Polymer Electrolytes. *Electrochimica Acta*. 52: 3181-3189. DOI: https://doi.org/10.1016/j.electacta.2006.09.70.

[17] Wu, T. T., Jahim, J. M., Muhammad, A. W., & Anuar, N. 2007. Palm Oil Mill Effluent (POME) Treatment and Bio Resources Recovery using Ultrafiltration Membrane: Effect of Pressure on Membrane Fouling. *Biochemcical Engineering Journal*. 35(3): 309-317. DOI: https://doi.org/10.1016/j.bej.2007.01.029.

[18] Yuliwati, E., and Ismail, A. F. 2011. Effect of Additives Concentration on the Surface Properties and Performance of PVDF Ultrafiltration Membranes for Refinery Produced Wastewater Treatment. *Desalination*. 273(1): 226-234. DOI: https://doi.org/10.1016/j.desal.2010.11.023.

[19] Oh, S. J., Kim, N., and Lee, Y. T. 2009. Preparation and Characterization of PVDF/TiO_2 Organic-inorganic Composite Membranes for Fouling Resistance Improvement. *Journal of Membrane Science*. 345: 13-20. DOI: https://doi.org/10.1016/j.memsci.2009.08.003.

[20] Arthanareeswaran, G., Mohan, D., and Raajenthiren, M. 2007. Preparation and Performance of Polysulfone-sulfonated Poly-(ether ether ketone) Blend Ultrafiltration Membranes. Part I. *Applied Surface Science*. 253: 8705-8712. DOI: https://doi.org/10.1016/j.apsusc.2007.04.053.

[21] Kukizaki, M., and Wada, T. 2008. Effect of The Membrane Wettability on the Size and Size Distribution of Microbubbles Formed from Shirasu-porous-glass (SPG) Membranes. *Journal Colloids and Surfaces A: Physicochem. Engineering Aspects*. 317: 146-154. DOI: https://doi.org/10.1016/j.colsurfa.2007.10.005.

[22] Jarma, Y. A., Parlar, I., Pek, T. O., Kayral, K., Kabay, K., Yigit, N. O., Kitis, M., & Yuksel, M. 2018. Study on Operational Conditions to Minimize Membrane Fouling in Membrane Bioreactor (MBR) System for Wastewater Treatment-preliminary Pilot Tests. *Journal of Membrane Science Research*. 4: 212-217. DOI: 10.22079/JMSR.2018.81330.1177.

[23] Lukina, A. O., Boutin, C., Rowland, O., and Carpenter, D. J. 2016. Evaluating Trivalent Chromium Toxicity on Wild Terrestrial and Wetland Plants. *Chemosphere*. 162: 355-366. DOI: https://doi.org/10.1016/j.chemosphere.2016.07.055.

[24] Bokhary, A., Tikka, A., Leitch, M., & Liao, B. 2018. Membrane Fouling Prevention and Control Strategies in Pulp And Paper Industry Appalication: A Review. *Journal of Membrane Science Research*. 4: 181-197. DOI: 10.22079/jmsr.2018.83337.1185.

[25] Eternadi, H., & Qazvini, H. 2020. Investigation of Alumina Nanoparticles Role on the Critical Flux and Performance of Polyvinyl Chloride Membrane in a Submerged Membrane System for the Removal Of Humic Acid. *Polymer Bulletin*. Springer Verlag GmbH. DOI: https://doi.org/10.1007/s00289-020-03234-z.

[26] Moustakes, N. G., Katsaros, F. K., Kontos, A. G., Ramanos, G. E., Dionysiou, D. D., & Falaras, P. 2014. Visible Light Active TiO_2 Photocatalytic Filtration Membranes with Improved Permeability and Low Energy Consumption. *Catalysis Today*. 224: 56-69. DOI: https://doi.org/10.1016/j.cattod.2013.10.063.

[27] Fane, A. G., Yeo, A., Law, A., Parameshwaran, K., Wicaksana. K., & Chen, V. 2005. Low Pressure Membrane Processes- Doing More with Less Energy. *Desalination*. 185: 159-165. DOI: https://doi.org/10.1016/j.desal.2005.04.039.

[28] Razmjou, A., Arifin, E., Dong, G., Mansouri, J., & Chen, V. 2012. Superhydrophobic Modification of TiO_2 Nanocomposite PVDF Membranes for Applications in Membrane Distillation. *Journal of Membrane Science*. 415-416: 850-863. DOI: https://doi.org/10.1016/j.memsci.2012.06.004.

[29] Dzinun, H., Ichikawa, Y., Honda, M., & Zhang, O. 2020. Efficient Immobilised TiO_2 in Polyvinylidene Fluoride (PVDF) Membrane for Photocatalytic Degradation of Methylene Blue. *Journal of Membrane Science Research*. 6: 188-195. DOI: 10.22079/JMSR.2019.106656.1263.

[30] Vanneste, J., Peumans, W. J., Van Damme, E. M. J., Darvishmanesh, S., Bernaderts, K., Geuns, J. M. C., Bruggen, B. V. 2014. Novel Natural and Biomimetic Ligands to Enhance Selectivity of Membrane Processes for Solute–solute Separations: Beyond Nature's Logistic Legacy. *Journal of Chemical Technology and Biotechnology*. 89: 354-371. DOI: https://doi.org/10.1002/jctb.4238.

[31] Li, X., Liu, Y., Jiang, H., & Chen, R. 2018. Computational Fluid Dynamics Simulation of a Novel Membrane Distributor of Bubble Columns for Generating Microbubbles. *Industry Engineering Chemical Research*. 58: 1087-1094. DOI: https://doi.org/10.1021/acs.iecr.8b05776.

[32] Martini, S., and Ang, H. M. 2019. Hybrid TiO_2/UV/PVDF Ultrafiltration Membrane for Raw Canola Oil Wastewater Treatment. *Desalination and Water Treatment*. 148: 51-59. DOI:10.5004/dwt.2019.23771.